Dalton Transactions

Accepted Manuscript

ROYAL SOCIETY OF CHEMISTRY

www.rsc.org/dalton

DFT study on the Reaction Mechanism of the Ring Closing Enyne Metathesis (RCEYM) Catalyzed by Molybdenum Alkylidene complexes

Xavier Solans-Monfort

Departament de Química, Universitat Autònoma de Barcelona, Edifici C_n

08193 – Bellaterra, Spain.

ABSTRACT

The ring closing enyne metathesis reaction (RCEYM) catalyzed by molybdenum based monoalkoxy pyrrolyl Schrock type catalysts has been studied by means of DFT (B3LYP-D) calculations. The two potential active alkylidene species as well as the three proposed reaction mechanisms (*ene-then-yne*, *endo-yne-then-ene* and *exo-yne-then-ene*) have been taken into account. Moreover, the influence in the *exo*- and *endo*-selectivity of the reactant substituents has also been explored. Results show that, in contrast to what is found for RCEYM processes catalyzed by Ru-based catalysts, the metallacyclobutene is a very short-living reaction intermediate that can be present in two isomeric forms (trigonal bipyramid (TBP) coordination around the metal center and square based pyramid (SPY) coordination). These two isomers are directly involved in the reaction mechanism and the ring opening takes place from the SPY species. Moreover and regardless of the nature of the reacting metal-alkylidene, the *yne-then-ene* pathways (*endo*- or *exo*-) are computed to present significantly lower energy barriers than the *ene-then-yne* pathway and thus the latter is computed not to take place. Finally, the *exo*-/*endo*- selectivity is predicted to highly depend on the sterics of the two carbon ends of the alkyne fragment. In this way, the carbon bearing the largest group prefers to interact with the carbon end of the metal-alkylidene. This places the bulkiest groups as far as possible of the metal fragment and overall leads to a generally lower energy barrier for the metallacyclobutene formation, the key step in defining the *exo*-/*endo*- selectivity.

INTRODUCTION

The enyne metathesis[1-4] is a derivative process of the well-known alkene metathesis reaction.[5-15] It refers to the atom economy reaction between an alkene and an alkyne molecule that leads to a 1,3-conjugated diene product (Scheme 1a). The intramolecular version of this process is known as ring closing enyne metathesis reaction (RCEYM) and it implies an enyne reactant that is converted to a cyclic conjugated 1,3-diene product (Scheme 1b).[1, 2, 4, 16-19] This latter reaction is seen as a powerful route in organic synthesis and it has been used for the synthesis of many different biologically relevant products.[14, 16] Noteworthy, RCEYM only takes place in presence of an appropriate catalyst and among all developed ones, the latest generations of Mo, W[20-22] and Ru-based alkene metathesis precatalysts[23-27] have been reported to be efficient (Scheme 2a). Complexes shown in scheme 2 are not the active species in the catalytic cycle as they do not present the carbene ligand leading to the final product. The real catalysts are achieved by the reaction of these precatalysts with a reacting molecule[28-32] and depending on the applying mechanism (see below) can lead to different active species. For instance, taking the species considered in this study (complex **1** (Scheme 2a) as precatalyst and **R1** (Scheme 1c) as reacting enyne), the expected active alkylidenes are complexes **I** and **II** (Scheme 2b).

The reaction can proceed through two different mechanisms that differ in the order in which the unsaturated fragments react with the metal center (Schemes 3 and 4):[20-27, 33-38] The *ene-then-yne* mechanism implies first the reaction of the alkene fragment; and the *yne-then-ene* pathway involves first the reaction with the alkyne. Evidences for the two mechanisms exist in the literature[20, 21, 23-27, 33] and nowadays it is well accepted that the applicability of one or other mechanism is highly dependent on the nature of

the catalysts, reactants and reaction conditions. Interestingly, reactions proceeding exclusively through the *ene-then-yne* mechanism leads to the formation of the product ***exo*-P**, which for the considered reactants (**R1** to **R7** in Scheme 5) presents a 5-membered ring (Scheme **1c** shows the ***exo*-P** product of **R1**). In contrast, reactions proceeding through an *yne-then-ene* mechanism can lead either to the formation of the ***exo*-P** or ***endo*-P** products depending on the relative orientation between the alkyne fragment and the metal complex in the initial alkyne skeletal rearrangement steps (Scheme **1c** shows the ***endo*-P** product of **R1**).[20, 21, 23, 25-27] The *exo*- and *endo*- term arises from the position of the cleaved triple bond in the final product (exocyclic or endocyclic respectively) and translates to a larger ring for the case of the *endo* product.

Figure 1 shows a selected list of some experimentally performed reactions involving enynes that lead to the formation of 5 or 6-membered ring conjugated dienes. These are the ring sizes potentially obtained with the model reactants used in the present work. Most precatalysts are normally selective to either the *exo*- or the *endo*- product. In particular, the Ru-based carbenes generally lead to the exclusive formation of the *exo* product,[1, 19, 23-27, 38] while the d^0 Schrock type catalyst preferentially forms the *endo* one.[20, 21] This suggests that the operating mechanism for these two type of catalysts is different and, while Ru-based catalyst could either proceed through the *ene-then-yne* or the *yne-then-ene* mechanism, the Mo or W-based complexes have to proceed exclusively through an *yne-then-ene* mechanism.

Several computational studies have been devoted to the study of the Ru,[39-55] Mo, W[56-68] or Re based[69-71] catalyzed alkene metathesis reactions and derivative processes.

They have shown the viability of the Chauvin mechanism[11, 72] either for early transition metal complexes and Ru-based catalysts and the key role of metallacyclobutane intermediates. In particular, studies focused on the reactivity of d^0 metal catalysts have shown that the mechanism consists in four elementary steps (alkene coordination, cycloaddition, cycloreversion and alkene decoordination) (Scheme 6a).[63, 66, 67, 69] The energetically preferred alkene coordination always takes place *trans* to the stronger σ-donor ligand (i.e. trans to the pyrrolyl in the most frequent monoalkoxy pyrrolyl (MAP) complexes). Moreover, within the two metallacyclobutane isomers (Scheme 6a),[73-79] only the one presenting a trigonal bipyramid structure (TBP) is involved directly in the productive pathway. The square based pyramid isomer (SPY) is usually more stable and thus it is considered as a resting state. Similarly, several studies on the alkyne metathesis reaction with Mo and W-based catalysts have been published in the literature.[61, 62, 64, 65] They have shown that the reaction mechanism is based on Katz mechanistic proposal[80] and it consists in three different steps: cycloaddition, metallacyclobutadiene rearrangement and cycloreversion (Scheme 6b). That is, the alkyne-complex has never been found to be a minimum on the potential energy surface and thus, the metallacyclobutadiene is formed in one single step process. Moreover and analogously to the alkene metathesis, for catalysts having different ancillary ligands, the alkyne coordination takes place *trans* to the stronger σ-donor group.[62, 64, 65]

In this work, we have explored the reactivity in ring closing enyne metathesis of Mo-based catalysts. Noteworthy, in contrast to the significant amount of theoretical contributions analyzing the enyne reaction with Ru-based catalyst,[44, 50, 81, 82] the reactivity of d^0 metal catalyst in RCEYM has never been explored computationally. In a

first part, the reactivity of the active species **I** and **II** (Scheme 2b) with **R1** (Scheme 5) as model of reactant through either the *ene-then-yne*, the *exo-yne-then-ene* or *endo-yne-then-ene* mechanism is considered. Based on previous results in the literature,[63, 66, 67, 69] we have limited the exploration to pathways in which the coordination of the unsaturated fragment takes place *trans* to the stronger σ-donor pyrrolyl ligand. In a second part, we considered the effects of reactant substituents (**R2** to **R7** enynes in Scheme 5) in the energy barrier height of the steps controlling the *endo-*/*exo-* selectivity. Results show that, in contrast to what is computed for Ru-based catalysts,[44, 50, 81, 82] the *ene-then-yne* mechanism is significantly disfavored and thus the reaction proceeds exclusively through an *yne-then-ene* mechanism. Moreover, although the small energy differences are on the limitations of the modeling approach, the calculations suggest that the *exo-*/*endo-* selectivity is mainly influenced by the bulk of the alkyne fragment substituents.

COMPUTATIONAL DETAILS

The methodology used in this study is similar to that used in the previous articles on Ru-based RCEYM reaction of our group.[81, 82] All geometry optimizations are performed with the B3LYP hybrid density functional.[83, 84] A 6-31G(d,p)[85, 86] basis sets is used for representing the main group elements. Molybdenum is represented with the Stuttgart-Bonn group pseudopotential[87] associated with the corresponding basis sets enlarged with a f polarization function.[88] The nature of the stationary points (minima or transition structure) is verified by vibrational analysis and the connectivity of the key transition structures is checked by performing the corresponding Intrinsic Reaction Coordinate (IRC) calculation. Energy refinement is made by performing single point

calculations using the larger 6-31++G(d,p)[89] basis sets for the main group elements. In these single point calculations, solvent effects (dichloromethane) are taken into account using the C-PCM continuum model.[90-92] The gas phase thermal corrections are evaluated with the smallest basis sets at 298.15 K and 1 atm. Moreover, since the role of non-covalent interactions has been shown to be relevant in many studies on alkene metathesis,[48, 51, 93] the effect of Dispersion forces is included with the D2 Grimme's empirical correction[94, 95] at the optimized geometries (S_6 = 1.05). Overall, the energies reported in the text are based on G_{gp} +ΔG_{solv} + D values and they include the thermal corrections at the gas phase (G_{gp}), solvent effects (ΔG_{solv}) and dispersion forces (D). All calculations are performed with Gaussian03[96] or Gaussian09[97] packages.

RESULTS AND DISCUSSION

Results are divided in three parts. First, the reactivity of the model enyne **R1** with **I** (Scheme 2b) either through an *yne-then-ene* (*exo*- or *endo*-) or and *ene-then-yne* mechanism is presented (Scheme 3). Noteworthy, the reactivity of **I** with **R1** through the *exo*- and *endo-yne-then-ene* pathways leads to the formation of the RCEYM products: ***exo*-P1** and ***endo*-P1** (Scheme 1c). In contrast, the reaction of **I** with **R1** through an *ene-then-yne* pathway interconverts the two active alkylidene species (**I** and **II**; Scheme 3a). In the second part, the reactivity of enyne **R1** with alkylidene **II** is discussed (Scheme 4). In this case, the *ene-then-yne* pathway leads to the formation of the ***exo*-P1** product (Scheme 4b), while the reactivity through the *yne-then-ene* pathway leads to the formation of dimeric products (Scheme 4a). In the final part, the effect of the reacting enyne substituents (**R2** to **R7** in Scheme 5) in the preference for

one or other pathway is discussed considering only the key transition structure in defining the *exo*-/*endo*- selectivity.

Reactivity of R1 with I through an yne-then-ene mechanism. Regardless the relative orientation of the reactant and the catalyst (*endo*- or *exo*- pathway) as well as the nature of the latter (**I** or **II**), the *yne-then-ene* mechanism is formed by two main processes: an intermolecular alkyne rearrangement that forms a conjugated alkylidene and an intramolecular ring closing alkene metathesis process (Figures 2 to 4). The former involves three steps: metallacyclobutene formation, metallacyclobutene rearrangement from a trigonal bipyramid coordination (TBP) to a square based pyramid one (SPY) and metallacyclobutene opening. As in the case of the alkyne metathesis reaction,[61, 62, 64, 65] the akyne-complex is not found as a minimum on the potential energy surface and thus there is no alkyne coordination step. Moreover, the metallacyclobutene is found to be a short-living intermediate that may be present in two isomeric forms (TBP and SPY). This is in contrast to what has been reported for RCEYM catalyzed by Ru-based complexes where the metallacyclobutene is not a minimum of the potential energy surface.[44, 50, 81, 82] This indicates a mechanistic difference between the two families of catalysts that does not seem to have big consequences in the overall reactivity as all energy barriers involving the metallacyclobutene rearrangements are low or very low (see below). Finally, four different steps can be identified in the intramolecular alkene metathesis process (alkene coordination, cycloaddition, cycloreversion and alkene decoordination). Nevertheless, for the intramolecular cases, the transition structure for the alkene coordination and/or decoordination steps have sometimes not been located. Since the reaction mechanisms are equivalent for all *yne-then-ene* pathways reported in the

present study, only the *endo-yne-then-ene* pathway involving the reaction of **I** with **R1** will be described in details. For all other cases, only the effects on the energetics of the different catalyst-reactant relative orientations or nature of the alkylidene will be pointed out. Figure 2 reports the energetics of the *endo-yne-then-ene* pathway and Figure 3 shows the geometries of the intermediates and transition structures.

For the *endo-yne-then-ene* mechanism, the metallacyclobutene formation from separated reactants occurs in a slightly exergonic step (ΔG = -0.6 kcal mol^{-1}) that has an associated energy barrier of 11.5 kcal mol^{-1}. The transition structure **endo-I-YTE-TS1-2** presents the metal, the imido, the alkoxy and the alkylidene groups essentially in the same plane. The M···$C_{terminal}$, M···$C_{internal}$ and $C_{carbene}$···$C_{internal}$ distances are 2.31, 2.56 and 2.57 Å, respectively. Intermediate **endo-I-YTE-2** presents a trigonal bipyramid metal center coordination (TBP) with apical imido and alkoxy ligands. The metallacyclobutene fragment is flat and the M-C_α distances are 2.06 and 2.08 Å, the C_α-C_β bond distances are 1.34 Å for the formal C=C double bond and 1.56 Å for the C-C single bond and the M···C_β distance is 2.37 Å. Therefore, although **endo-I-YTE-2** presents a rather short M···C_β distance as it is the case for TBP metallacyclobutane intermediates,[73-79] the bond distances between C_α and C_β carbons are within those expected for usual C-C and C=C bonds and thus they are not elongated as observed in metallacyclobutane intermediates.[57, 63, 66, 67, 69, 73, 75, 76, 78, 79]

The TBP metallacyclobutene intermediate can further evolve to a more stable SPY isomer (**endo-I-YTE-3**) with the imido ligand in apical position. The reaction Gibbs energy is strongly exergonic (-15.3 kcal mol^{-1}) and the energy barrier with respect to **endo-I-YTE-2** is only 5.6 kcal mol^{-1}. Noteworthy, the stabilization of the SPY isomer

with respect to TBP intermediate is much larger than those traditionally reported for molybdenum imido metallacyclobutane intermediates,[63, 66, 67] suggesting that **endo-I-YTE-3** intermediate should have an active role in the reaction. The SPY metallacyclobutene intermediate presents a less flat metallacyclobutene fragment (Ω = 18.6º) than the TBP isomer and a longer M···C_β distance of 2.67 Å. These features are similar to those reported for SPY metallacyclobutanes.[73-76] Moreover, the M-C_α distances are longer and much more assymetrical than for **endo-I-YTE-2** (2.11 Å for the M-C_α involving the carbon coming originally from the enyne and 2.24 Å for the M-C_α involving the carbon of the alkylidene).

At this point it is worth mentioning that a transition structure connecting directly separated reactants with the SPY metallacycle was not found despite the efforts to locate it. The scan along the M···C_{yne} distances showed a maximum that when allowed to fully relax as a transition structure evolved to the transition structure associated with the formation of the TBP isomer. This could be due to the smaller *trans* influence of the imido ligand when compared with the alkylidene that forces a wide alkoxy-molybdenum-imido angle that evolves to the TBP metallacyclobutene isomer.

From **endo-I-YTE-3** a transition structure associated with the elongation of the M-C_α bond involving the original carbon of the alkylidene leads to a 1,3-conjugated carbene. The reaction Gibbs energy of this process is again strongly exergonic (ΔG = -12.5 kcal mol^{-1}) and, remarkably the corresponding Gibbs energy barrier is very small (ΔG = + 2.8 kcal mol^{-1}). The M-C_α distances, the C_α-C_β bonds and the C_β-C_α-M-N_{imido} torsional angle are between the values of **endo-I-YTE-3** and **endo-I-YTE-4** suggesting a significant electronic reorganization. The **endo-I-YTE-4** presents geometrical features

equivalent to those of other Mo alkylidenes: a M-$C_{carbene}$ distance of 1.91 Å and a coplanar rearrangement of the alkylidene substituents and the imido group. The **endo-I-YTE-4** intermediate involved in the reaction pathway corresponds to the *anti* isomer (alkylidene substituents pointing opposite to the imido ligand). Nevertheless, the related *syn* isomer, with the alkylidene substituents pointing towards the imido, is lower in energy by 1.8 kcal mol^{-1}.

Overall, the intermolecular alkyne rearrangement leading to a conjugated alkylidene is strongly favorable ΔG = -28.4 kcal mol^{-1} and requires overcoming relatively small energy barriers. In fact, once the TBP metallacyclobutene intermediate has been formed all Gibbs energy barriers are small and thus the energy barrier limiting this *endo-yne-then-ene* pathway is that associated with the cycloaddition ($\Delta G^{\neq}$ = + 11.5 kcal mol^{-1} with respect to separated reactants). This is similar to what has been computed for the ring closing metathesis reaction catalyzed by Ru-based complexes,[44, 50, 81, 82] the main difference being that in the present case the metallacyclobutene is a short-living intermediate that rearranges from TBP to SPY and then to the conjugated carbene.

From the metal-alkylidene complex **endo-I-YTE-4**, the intramolecular alkene metathesis process takes place. It is worth mentioning, first, that the alkene-complex (**endo-I-YTE-5**) is not located as a minimum on the potential energy surface for the *endo-yne-then-ene* pathway and in fact, the IRC associated with **endo-I-YTE-TS4-6** evolved to a conformer of the **endo-I-YTE-4** alkylidene with no interaction between the metal and the alkene fragment. As a consequence, the calculations suggest that the metallacyclobutane formation occurs in one single step in the *endo-yne-then-ene* pathway, but in two steps in the *exo-yne-then-ene* pathway (see Figure 4). The energy

barriers for the alkene coordination and cycloaddition with respect to the **exo-I-YTE-5** complex of the *exo-yne-then-ene* route are really small (2.3 and 0.9 kcal mol^{-1} respectively) and thus, for this particular case, the fact that the process is one or two steps does not seem to influence significantly the overall reactivity.

The one step cycloaddition is slightly endergonic and it presents a low energy barrier (**endo-I-YTE-TS4-6**). The reaction Gibbs energy is 3.6 kcal mol^{-1} and **endo-I-YTE-TS4-6** is located 6.1 kcal mol^{-1} above the metal-alkylidene complex. The metallacyclobutane intermediate has a trigonal bipyramid (TBP) coordination around the metal center with apical imido and alkoxy groups. As expected, a SPY metallacyclobutane isomer has also been found to be a minimum of the potential energy surface (**endo-I-YTE-6SPY**). It is 7.6 kcal mol^{-1} lower in energy than the TBP intermediate. However, according to previous calculations, this SPY isomer is not involved in the alkene metathesis pathway[60, 66, 67] and, for this particular case, the transition structure connecting the TBP and SPY isomers has essentially the same Gibbs energy than that of cycloreversion from **endo-I-YTE-6**. Therefore, the cycloreversion from **endo-I-YTE-6SPY** has not been explored. The cycloreversion and alkene decoordination from **endo-I-YTE-6** takes place in a single step that implies a Gibbs energy barrier of 9.0 kcal mol^{-1} wih respect to the TBP metallacyclobutane. Therefore, the intramolecular alkene metathesis reaction from **endo-I-YTE-4** requires overcoming energy barriers that are slightly higher than those associated with the intermolecular alkyne skeletal reorganization. The energy difference between the lowest in energy intermediate (**endo-I-YTE-4**) and the highest in energy transition structure (**endo-I-YTE-TS6-I**) of the alkene metathesis part is 12.6 kcal mol^{-1} (16.6 kcal mol^{-1} from **endo-I-YTE-6SPY**). Nevertheless, the high exergonicity

of the alkyne fragment rearrangement reaction (irreversible process) indicates that the alkene metathesis reaction has no influence in defining the *endo*-/*exo*- selectivity.

Very similar energetics are obtained for the *exo-yne-then-ene* pathway (Figure 4). Again, the intermolecular alkyne skeletal reorganization is globally strongly exergonic and thus it is key in defining the viability of the *exo-yne-then-ene* pathway. However, the initial metallacyclobutene formation is only marginally favorable (ΔG = -2.0 kcal mol^{-1}) and thus the large exergonicity arises from the TBP to SPY rearrangement (ΔG = -10.9 kcal mol^{-1}) and from the SPY to conjugated alkylidene step (ΔG = -15.0 kcal mol^{-1}). The energy barriers associated with these three steps are relatively low and the one associated with the metallacyclobutene formation ($\Delta G^{\neq}$ = 10.8 kcal mol^{-1} with respect to separated reactants) corresponds to the highest in Gibbs energy transition structure. Concerning the ring closing alkene metathesis process (**exo-I-YTE-4** to **I** + **exo-P1**), it is found that all intermediates and transition structures are well below reactants in terms of Gibbs energies and thus, this process has no effect on determining the *exo*-/*endo*- selectivity. Noteworthy, for the *exo-yne-then-ene* pathway, the SPY isomer (**exo-I-YTE-6SPY**) of the metallacyclobutane intermediate is higher in Gibbs energy than the TBP intermediate by 5.6 kcal mol^{-1} and the transition structure connecting the two metallacyclobutane isomers is also higher in Gibbs energy than the transition structure for cycloreversion. Therefore, the **exo-I-YTE-6SPY** species is not expected to have a significant role in the reaction. This **exo-I-YTE-6SPY** species presents a puckered structure with the C_β carbon pointing away the imido ligand, a conformation that has not been located in the calculations of unsubstituted metallacycles with small models.[63, 66, 67] Overall, the most stable intermediate of the

ring closing metathesis process is the TBP metallacycle isomer and the energy difference between the lowest intermediate (**exo-I-YTE-6**) and the highest transition structure (cycloreversion) is 12.4 kcal mol^{-1}. Therefore, the energy barrier defining the feasibility of the *exo-yne-then-ene* pathway is that associated with the metallacyclobutene formation of the alkyne skeletal reorganization (**exo-I-YTE-TS1-2**), and the rate limiting process is the intramolecular alkene metathesis. The **exo-I-YTE-TS1-2** transition structure is located 10.8 kcal mol^{-1} above separated reactants and the energy span of the intramolecular alkene metathesis process is 12.4 kcal mol^{-1}. These values are similar to that obtained for the *endo-yne-then-ene* route.

Reactivity of R1 with I through an ene-then-yne mechanism. The reaction of **R1** with **I** through an *ene-then-yne* mechanism implies first a cross metathesis process leading to the formation of alkylidene **I-ETY-5** and, afterwards, an intramolecular alkyne fragment rearrangement that forms the conjugated alkylidene **II** (Figure 5). Therefore, the process interconverts **I** into **II**. The number and nature of steps is essentially the same to the *yne-then-ene* pathways but in this case they take place in opposite order. The cross metathesis process implies four steps: alkene coordination, cycloaddition, cycloreversion and ethene decoordination (Figure 5) and the alkyne rearrangement implies three steps: formation of the TBP metallacyclobutene intermediate, TBP to SPY metallacyclobutene rearrangement and formation of the conjugated alkylidene.

The cross metathesis process starts with a significantly endergonic alkene coordination step (ΔG = 9.5 kcal mol^{-1}) that implies overcoming an energy barrier of 14.4 kcal mol^{-1}. Once the alkene-complex **I-ETY-2** is formed, this can react leading to the formation of the metallacyclobutane intermediate **I-ETY-3**, which is 1.8 kcal mol^{-1} above separated

reactants. Therefore, the metallacycle is slightly higher in energy than separated reactants, similarly to what has been recently pointed out by Hoveyda and co-workers.[68] The Gibbs energy barrier for the cycloaddition step is 6.5 kcal mol^{-1} and thus, **I-ETY-TS2-3** becomes the highest in Gibbs energy transition structure (rate determining transition structure) of the whole alkene metathesis process ($\Delta G^{\neq}$ = 16.0 kcal mol^{-1} with respect to separated reactants). The usually more stable square based pyramid metallacyclobutane intermediate (**I-ETY-3SPY**) is also found as a minimum of the potential energy surface. Nevertheless, as in the case of **exo-I-YTE-6SPY** of the *exo-yne-then-ene* pathway, it is slightly higher in energy ($\Delta G_{TBP\text{-}SPY}$ = +1.2 kcal mol^{-1}) and its formation from the TBP isomer is higher in Gibbs energy than the cycloreversion. Therefore, it is not expected to have an important role in the full process. Finally, the two mirror steps that lead to the formation of **I-ETY-5**, cycloreversion and ethene decoordination, are easier. In fact, **I-ETY-TS4-5** is not localized due to the very flat potential energy surface. From **I-ETY-5,** the intramolecular alkyne skeletal reorganization is strongly exergonic (ΔG = -39.4 kcal mol^{-1}) and all energy barriers are significantly lower than those of the cross metathesis process suggesting that once **I-ETY-5** is formed the reaction occurs easily leading to **II**.

Overall, the cross metathesis process interconverting **I** to **I-ETY-5** is key in determining the feasibility of the *ene-then-yne* process. Globally, the process is slightly endergonic (ΔG = 2.6 kcal mol^{-1}) and requires overcoming transition structures that are up to 16.0 kcal mol^{-1} above separated reactants. These energy barriers are not really high but they indicate that the *ene-then-yne* pathway is significantly less favored that both the

endo-yne-then-ene (11.5 kcal mol^{-1}) and *exo-yne-then-ene* (10.8 kcal mol^{-1}) processes. Calculations suggest that the *ene-then-yne* pathway from **I** does not occur.

The cross metathesis between **I** and the ***exo*-P** olefin can also interconvert **I** into **II**. It is for this reason that its feasibility has also been explored (Figure S1 of the Supplementary Information). For this reaction, the lowest in energy minimum are separated reactants and the highest in Gibbs energy transition structure is found to be the initial alkene coordination step. The Gibbs energy span is 16.4 kcal mol^{-1} a value very similar to that computed for reaction of **I** with **R1** through the *ene-then-yne* pathway. Therefore, this process will also rarely take place.

Reactivity of R1 with II (ene-then-yne and yne-then-ene pathways). As already mentioned above, the reaction of **R1** with **II** through and *ene-then-yne* leads to the formation of the ***exo*-P1** product. In contrast, the **R1** with **II** reaction through an *yne-then-ene* mechanism leads to the formation of dimeric species (Scheme 4). As expected, changing the nature of the reacting alkylidene does not have an effect on the number and nature of the elementary steps. Therefore the *ene-then-yne* pathway is formed by a cross metathesis process that occurs in four steps (alkene fragment coordination, cycloaddition, cycloreversion and alkene decoordination) and an intramolecular alkyne skeletal reorganization that takes place in three steps (metallacyclobutene formation, TBP to SPY isomerization and ring opening) (Figure 6). On the other hand, the *yne-then-ene* pathway involves first the strongly exergonic intermolecular alkyne skeletal reorganization that implies the same three steps described for the reaction between **R1** and **I** and then a intramolecular ring closing alkene metathesis process (Figure 7).

Figure 6 shows the energetics of the reaction of **R1** with **II** through the *ene-then-yne* mechanism. The overall cross metathesis process leading to the formation of **II-ETY-5** is slightly endergonic with a reaction Gibbs energy of 3.7 kcal mol^{-1}. It involves overcoming energy barriers that are in all cases lower than 16.0 kcal mol^{-1} for each individual step and the highest in free energy transition structure is that associated with the alkene decoordination. Moreover, all intermediates (alkene-complexes **II-ETY-2** and **II-ETY-4** and TBP (**II-ETY-3**) and SPY (**II-ETY-3SPY**) metallacycles) are significantly higher in Gibbs energies than separated reactants. The lowest one is **II-ETY-3SPY** that has a puckered metallacyclobutane fragment with the C_β pointing toward the imido and an energy relative to separated reactants of + 5.5 kcal mol^{-1}. However, this species is not directly involved in the productive pathway and its formation requires overcoming energy barriers that are higher than those of the productive pathway and thus it is not expected to have a significant role in the overall process. In any case, the energy difference defining the Gibbs energy cost for the alkene metathesis process is that between separated reactants and the alkene decoordination transition structure, which is equal to 19.3 kcal mol^{-1} (3.3 kcal mol^{-1} higher than that of the reaction between **R1** and **I**). The subsequent alkyne skeletal reorganization is strongly exergonic (ΔG = -40.3 kcal mol^{-1}) and it implies lower energy barriers. Therefore, the feasibility of the *ene-then-yne* mechanism is determined again by the cross metathesis process and the Gibbs energy span between the lowest intermediate (separated reactants) and the highest transition structure (alkene decoordination) is 19.3 kcal mol^{-1}.

The reactivity of **R1** with alkylidene **II** through the *yne-then-ene* mechanism (Figure 7) presents a strongly exergonic alkyne skeletal reorganization (ΔG = -22.8 kcal mol^{-1}).

However, in the present case, this exergonicity arises only from the last ring opening step. Going into details, it is found that the metallacyclobutene formation is slightly endergonic with a reaction Gibbs energy of +1.1 kcal mol^{-1} and an Gibbs energy barrier of 7.5 kcal mol^{-1}. The TBP to SPY interconversion is marginally exergonic (ΔG = -4.7 kcal mol^{-1}) and it requires to overcome the highest in Gibbs energy transition structure of the alkyne skeletal reorganization. This transition structure is located 8.3 kcal mol^{-1} above separated reactants. From the **II-YTE-3** intermediate, the SPY metallacyclobutene opening is highly favorable (ΔG = -19.1 kcal mol^{-1}) which leads to an overall irreversible process.

The subsequent intramolecular alkene metathesis implies three steps and their nature is equivalent to that of those described for the reaction of **I** with **R1** through the *exo*- and *endo-yne-then-ene* pathways. As in those cases, the transition structure located at higher Gibbs energies is that of the final cycloreversion step (**II-YTE-TS6-I**) and the computed Gibbs energy barriers suggest a feasible process. The energy span between **II-YTE-6** and **II-YTE-TS6-I** is 12.7 kcal mol^{-1}. Comparing the *ene-then-yne* and the *yne-then-ene* pathways starting from **II**, the computed energy values indicate that if **II** were present in the reaction mixture it would preferentially react through an *yne-then-ene* mechanism ($\Delta G^{\neq}$ = 8.3 kcal mol^{-1}) and not through the *ene-then-yne* route ($\Delta G^{\neq}$ = 19.3 kcal mol^{-1}). Therefore, this would form alkylidenes having two units of the reactants and probably deactivate the catalyst.

As already summarized in the introduction, the d^0 based alkylidene complexes able to perform the ring closing enyne metathesis produce selectivily the *endo* product (Figure 1). This is indicative that the applying mechanism is the *yne-then-ene* pathway.[20-22]

Only for some specific cases, some amounts of the *exo* product are detected.[20, 21] This could be attributed to the fact that in these cases the *exo-yne-then-ene* mechanism can be competitive, which would suggest relative small energy differences between the key energy barriers of the *endo-* and *exo-yne-then-ene* pathways. The calculations support, at least partially, these findings. The *endo-* and *exo-yne-then-ene* pathways starting from **I** as active allkylidene implies overcoming transition structures that are at least 4.5 kcal mol^{-1} lower in Gibbs energy than the highest transition structures of the *ene-then-yne* pathway. This energy difference is not very large but it is sufficient to explain the observed preference for the *yne-then-ene* pathway.[98] Similarly, the most feasible reactivity of **R1** with **II** is through the *yne-then-ene* pathway. The *yne-then-ene* preference for the reaction of **II** is of about 8.4 kcal mol^{-1}, which suggests that even if **II** were formed the *ene-then-yne* pathway leading to the ***exo*-P1** product would not take place.

This general preference for the *yne-then-ene* pathway was also observed for the reactivity of **R1** with Ru-based catalysts using the same computational approach,[81, 82] but in that case the energy differences between the two competitive processes were computed to be significantly lower (2.4 kcal mol^{-1}). This suggests that the applying mechanism is dependent on the nature of the reactants in the case of the Ru-based catalyst (specially the presence of substituents in the propargylic position favor the *ene-then-yne* pathway), but, in contrast, for Mo catalyst, the reaction should more likely exclusively proceed through an *yne-then-ene* mechanism.

The present calculations are not able to distinguish between the *endo-* and *exo-*selectivity for **R1**, as the *exo-yne-then-ene* (and not the *endo-yne-then-ene*) pathway is

preferred by 0.7 kcal mol^{-1}. However, despite this disagreement, an exploration on how the effect of the substituents can influence the metallacyclobutene formation energy barrier both for the *endo*- and *exo*-*yne*-*then*-*ene* pathway has been undertaken with the aim of analyzing how steric and electronic properties may influence the *endo*- and *exo*- selectivity, even assuming the limitations of the calculations.

Effect of reactants substituents. Reactivity of II with R2 to R7 enynes. With the aim of evaluating the effect of changing enyne reactant substituents, the energy barrier of the metallacyclobutene formation for the series of **R2** to **R7** enynes (Scheme 5) has been computed. According to present calculations, the transition structure associated with this step is key in determining the *endo*-/*exo*- selectivity and thus, the analysis of the effect of substituents in it should rationalize in a large extend the origin of the catalyst selectivity. It is worth mentioning that the considered reactants have been selected as illustrative examples for analyzing both the steric (-H vs. -CH_3, -*t*Bu) and electronic effects (-CH_3 vs. –F).

Table 1 summarizes the Gibbs energy barrier for the metallacyclobutene formation step for all considered reactants and pathways (*endo*- and *exo*-), as well as the Gibbs energy difference between the two routes. At first glance and taking the Gibbs energy barrier heights of **R1** as reference, it is observed that increasing the sterics of the reacting enyne (**R1** vs. **R2** to **R7**) produces a general increase of the energy barrier, the associated values ranging between 11.7 and 18.4 kcal mol^{-1}. Noteworthy, this trend is only marginally affected by the electronic nature of the substituents and thus, sterics are clearly the main factor.

Interestingly, the energy barrier increase is not equal for the two potential enyne – catalyst relative orientations. In this view, increasing the bulk of the substituents in the terminal position -H < -CH_3 < -CF_3 or -*t*Bu produce a significant increase of the energy barrier associated with the *endo-yne-then-ene* pathway from 11.5 to 13.1 and from 13.1 to 18.4 or 18.0 kcal mol^{-1}. In contrast, this energy barrier height increase is much less pronounced for the *exo-yne-then-ene* pathway, the associated values being 10.8, 12.0, 14.8 and 12.9 kcal mol^{-1} for –H, -CH_3, -CF_3 and -*t*Bu respectively. Consequently, for internal alkyne fragments, *the exo-yne-then-ene* mechanism is computed to be significantly preferred within the present methodology which tends to underestimate the viability of the *endo-yne-then-ene* pathway.

On the other hand, the effects on the energy barrier for the metallacyclobutene formation induced by substituents in the propargylic position are only significant for the *exo-yne-then-ene* pathway. In this way, substituting the –H (**R1** and **R3**) atoms by –F (**R5**) or –CH_3 (**R2** and **R4**) groups produce a not negligible increase of the metallacyclobutene formation energy barrier of the *exo-yne-then-ene* pathway that goes from 10.8 or 12.0 kcal mol^{-1} to 16.9, 13.7 and 13.9 kcal mol^{-1}, respectively. Overall, this leads to a preference for the *endo-yne-then-ene* pathway when the enyne has a terminal alkyne fragment and substituents in the propargylic position and this suggests again that sterics has a crucial role in favoring one or the other route.

In summary and assuming that the calculations underestimate the viability of the *endo-yne-then-ene* pathway with respect to the *exo-yne-then-ene* route, the present work outlines that the *endo-*/*exo-* selectivity in Mo-based catalysts seems to be highly influenced by the sterics of the reacting enyne. That is, although there is a small

electronic effect of the substituents, the preference for the one or other route seems to arise from the fact that in the **YTE-TS1-2** transition structure the preferred relative orientation between the reacting enyne and the metal fragment implies that the carbon of the triple bond bearing the largest groups interacts with the carbon end of the alkylidene. In this orientation, the bulkiest group points away from the rest of the complex and it further evolve to a metallacyclobutene where the carbon bearing the biggest substituents is in β position and thus far from the metal center. In this way, terminal alkyne fragments would lead mainly to *endo*- products and internal alkyne fragments could lead to a mixture of *exo*- and *endo*- products, the major one being, at least in part, related to the relative bulk of the two ends. Noteworthy, this is significantly different to what was proposed for Ru-based catalysts for which a larger influence of the electronic nature of the substituents was proposed.[81, 82]

CONCLUSIONS

The ring closing enyne metathesis reaction (RCEYM) catalyzed by molybdenum monoalkoxy pyrrolyl (MAP) Schrock type catalyst has been studied by means of DFT (B3LYP-D) calculations. The three proposed mechanisms for RCEYM reactions, *endo-yne-then-ene*, *exo-yne-then-ene* and *ene-then-yne*, as well as the two potential active alkylidene (**I** and **II** in Scheme 2) have been considered. The results show significant differences with previous computational works on RCEYM processes catalyzed with Ru-based complexes in agreement with the experimentally observed differences between the two families of catalysts.

Regarding the number and nature of the elementary steps of the reaction mechanism, it is worth highlighting that the intermolecular alkyne skeletal reorganization is found

to take place in three steps: metallacyclobutene formation; trigonal bipyramid (TBP) to square based pyramid (SPY) metallacyclobutene rearrangement and ring opening from the SPY isomer. Therefore, metallacyclobutenes are computed to be very short-living intermediates that can be present in two isomeric forms: TBP and SPY.

With respect to the energetics, calculations show that regardless of the alkylidene nature (**I** and **II**), the *yne-then-ene* pathways are computed to have overall significantly lower energy barriers than those of the *ene-then-yne* mechanism and thus, this indicates that the *ene-then-yne* pathway does not take place. This is in contrast to what has been previously found for RCEYM processes catalyzed with Ru-based complexes for which the *ene-then-yne* and *yne-then-ene* pathways have similar energetics and thus the applicability of one or other pathway depends on the nature of the reactants and reaction conditions. Finally, results highlight that the *endo*-/*exo*-selectivity is strongly influenced by the sterics of the reacting enyne. In this way, enynes having a bulky skeleton and a terminal alkyne fragment would lead to the *endo*- product. On the other hand, enynes with internal alkyne fragments would probably lead to mixtures of *endo*-/*exo*- products that seem to be highly dependent on the bulk of the two carbon ends of the alkyne group. This is attributed to the fact that the preferred mechanism is the one in which the most hindered carbon of the alkyne fragment interacts with the carbon end of the alkylidyne, placing the bulkiest groups as far as possible of the metal fragment.

ACKNOWLEDGEMENTS. Financial support from MICINN (CTQ2011-24847/BQU) and the Generalitat de Catalunya (SGR2009-638) is gratefully acknowledged.

SUPLEMENTARY INFORMATION. Figure S1 showing the energy profile of the reaction between **I** and ***exo*-P** olefin.

Table 1. Gibbs (G_{gp} + ΔG_{solv} + D) energy barriers ($\Delta G^{\neq}$) associated with the metallacyclobutene formation step of the *endo*- and *exo-yne-then-ene* pathway. Energy Difference ($\Delta(\Delta G^{\neq})$) between these two Gibbs energy barriers. All values are in kcal mol^{-1}.

	$\Delta G^{\neq}$		$\Delta(\Delta G^{\neq})$[a]
	endo-	*exo*-	
R1	11.5	10.8	+0.7
R2	11.7	13.7	-2.0
R3	13.1	12.0	+1.1
R4	12.5	13.9	-1.4
R5	18.0	12.9	+5.1
R6	15.6	16.9	-1.3
R7	18.4	14.8	+3.6

[a] a negative values indicates that the *endo-yne-then-ene* route is preferred over the *exo-yne-then-ene* one.

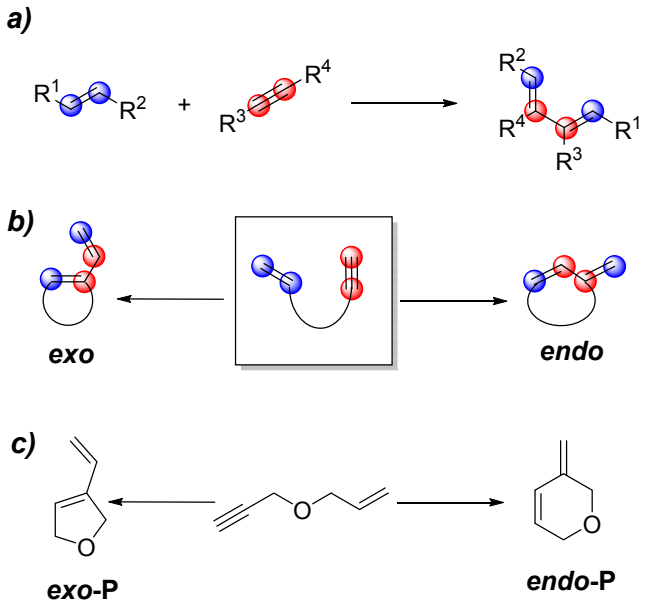

Scheme 1.

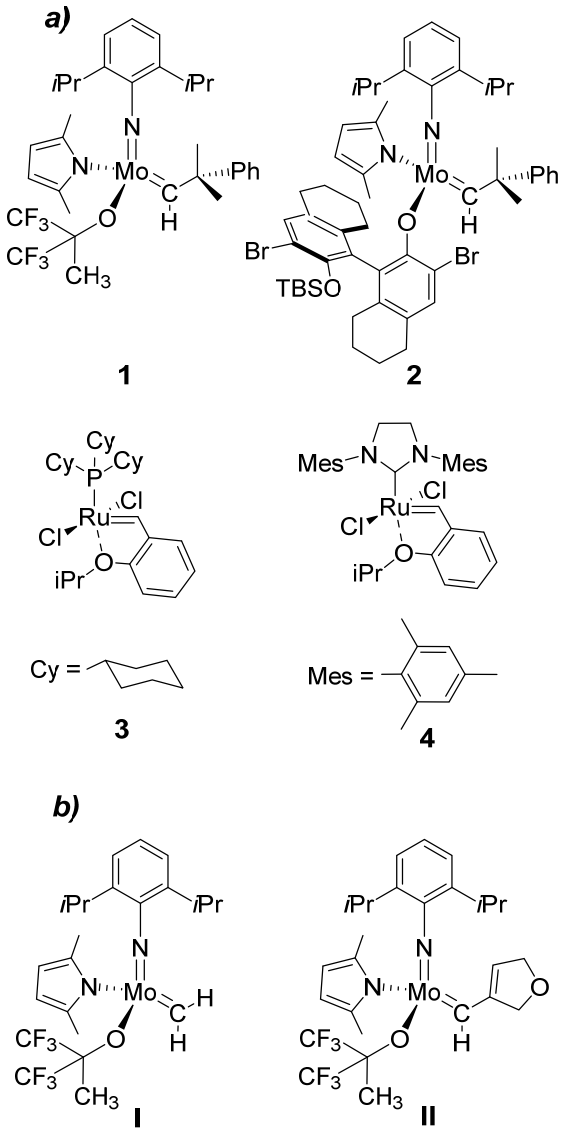

Scheme 2.

a) Reactivity of I through an ene-then-yne mechanism

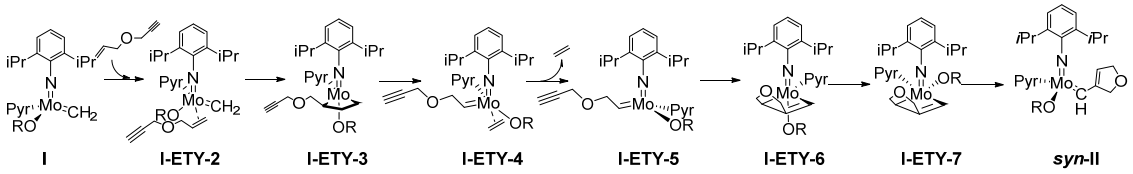

b) Reactivity of I through an exo-yne-then-ene mechanism

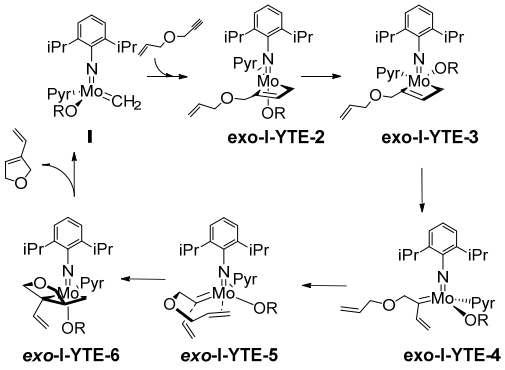

c) Reactivity of I through an endo-yne-then-ene mechanism

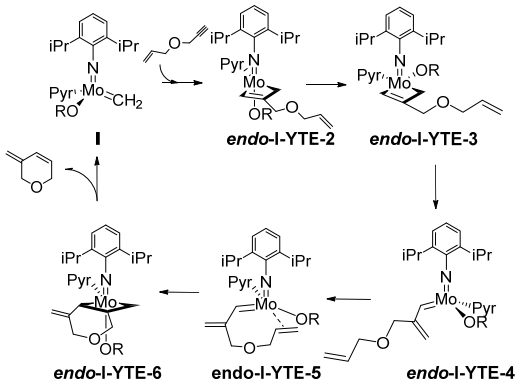

Scheme 3.

a) Reactivity of II through an yne-then-ene mechanism

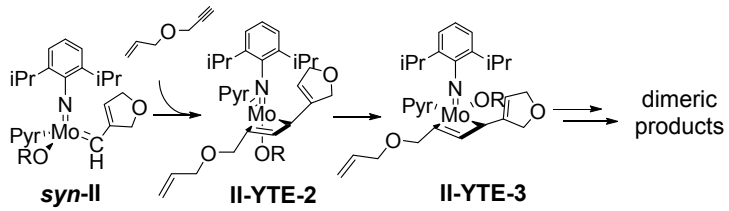

b) Reactivity of I through an ene-then-yne mechanism

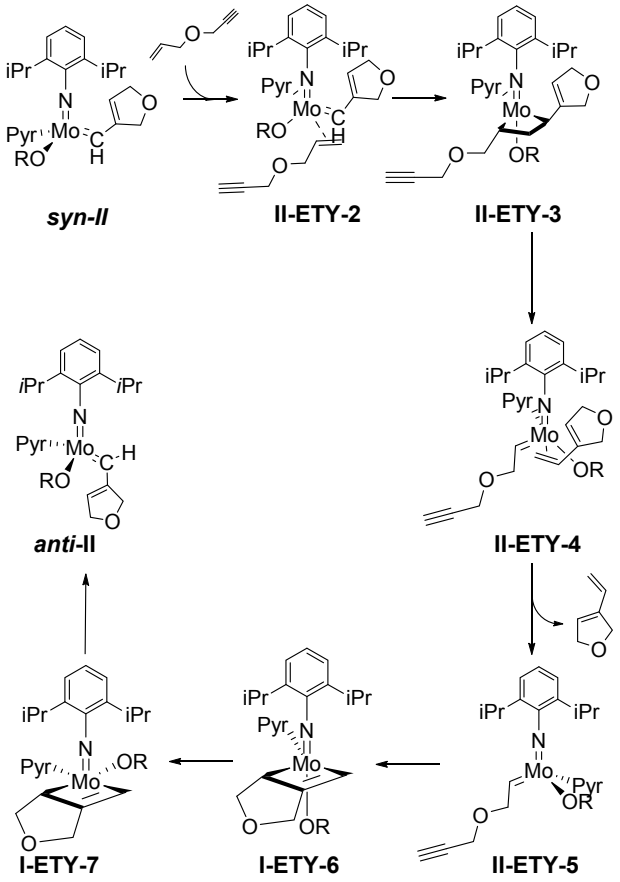

Scheme 4.

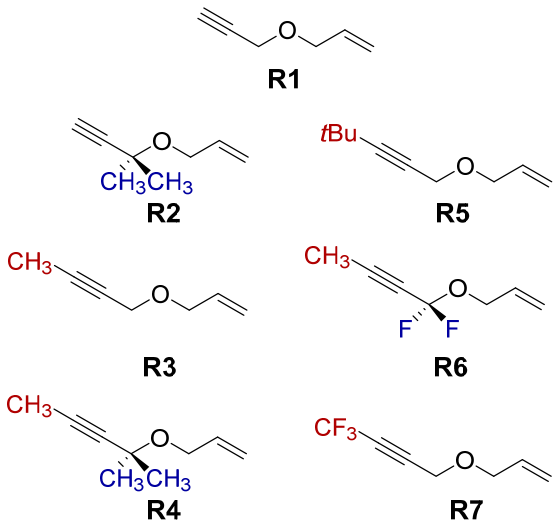

Scheme 5.

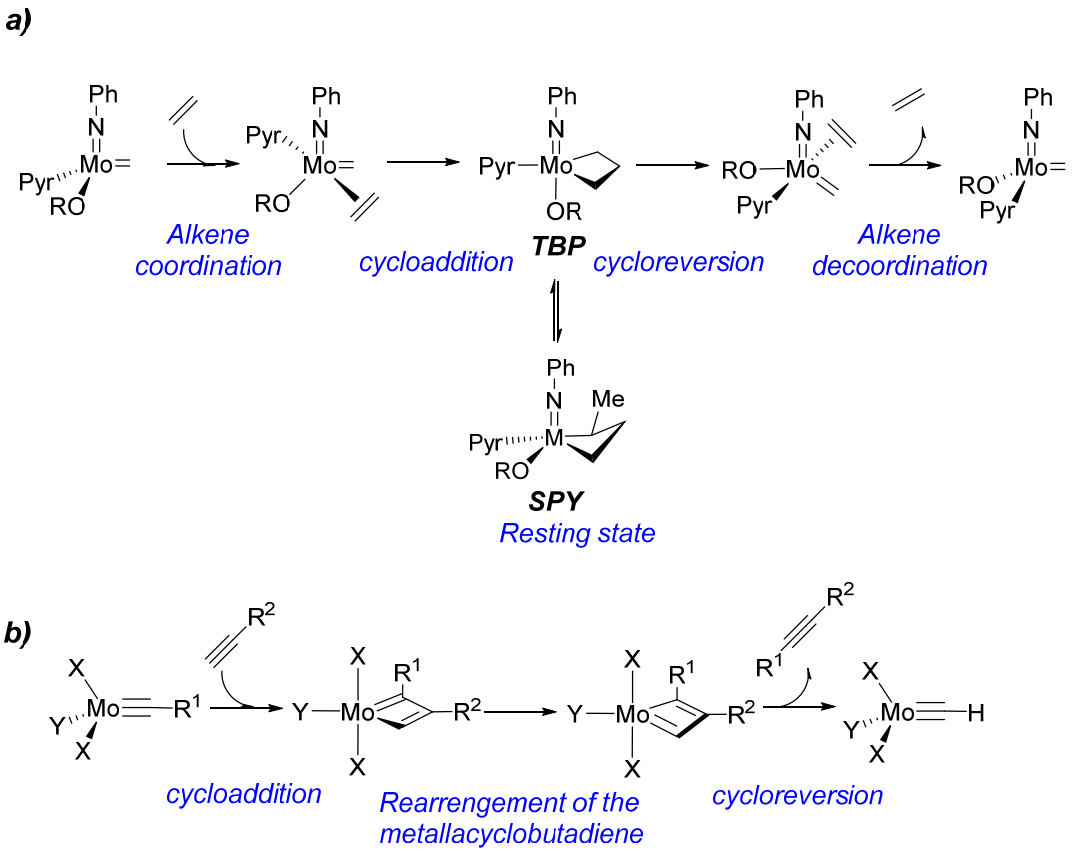

Scheme 6.

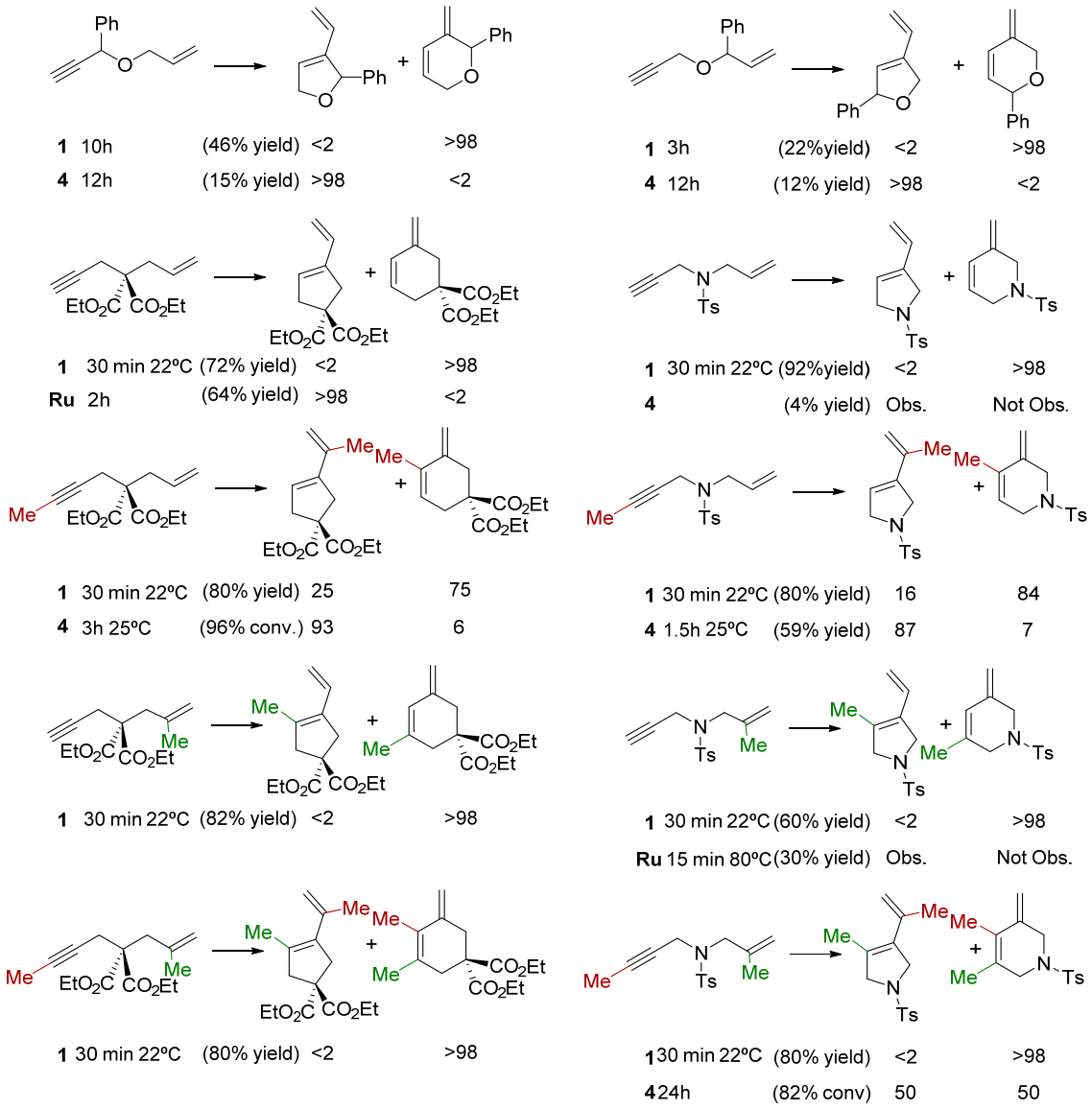

Figure 1. Reaction yields and *exo-/endo-* selectivity for some selected examples obtained experimentally with Mo (complex **1**) and Ru-based (mostly with complex **4**) catalysts (see Scheme 2 for complex definition). The data is extracted from references 20, 23, 26 and 27.

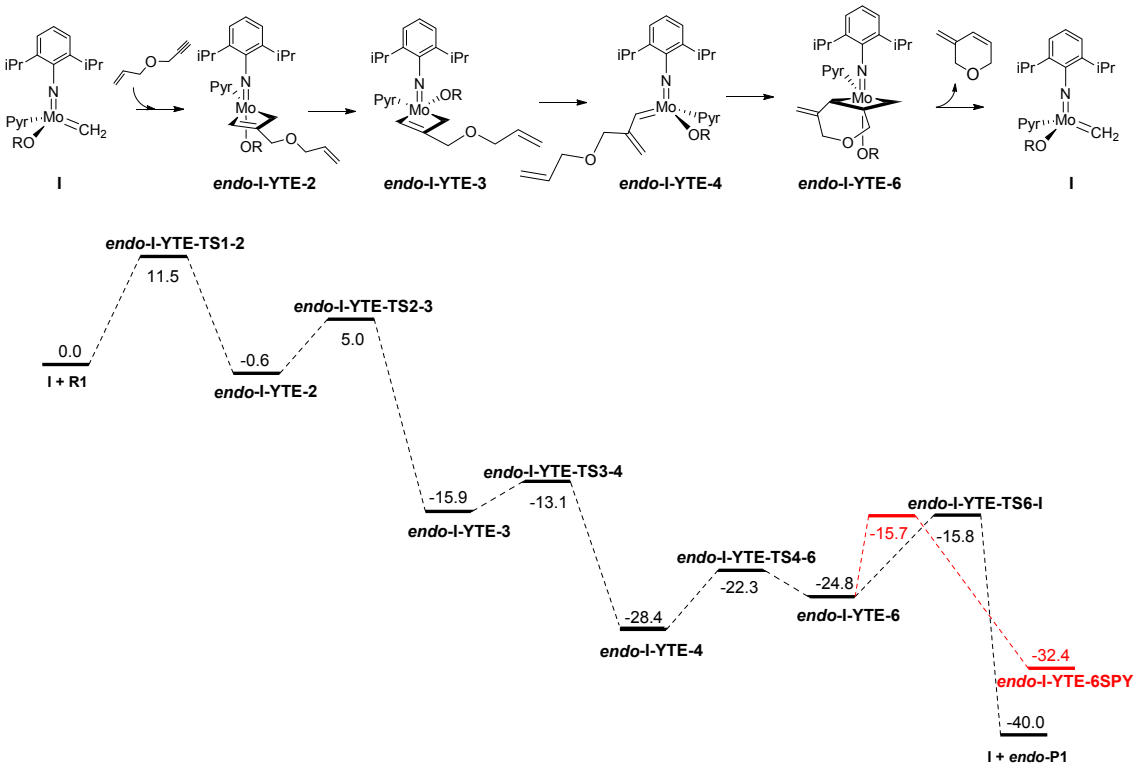

Figure 2. Gibbs energy profile (based on G_{gp}+ ΔG_{solv} + D in kcal mol^{-1}) for the reaction of alkylidene **I** with **R1** through the *endo-yne-then-ene* pathway.

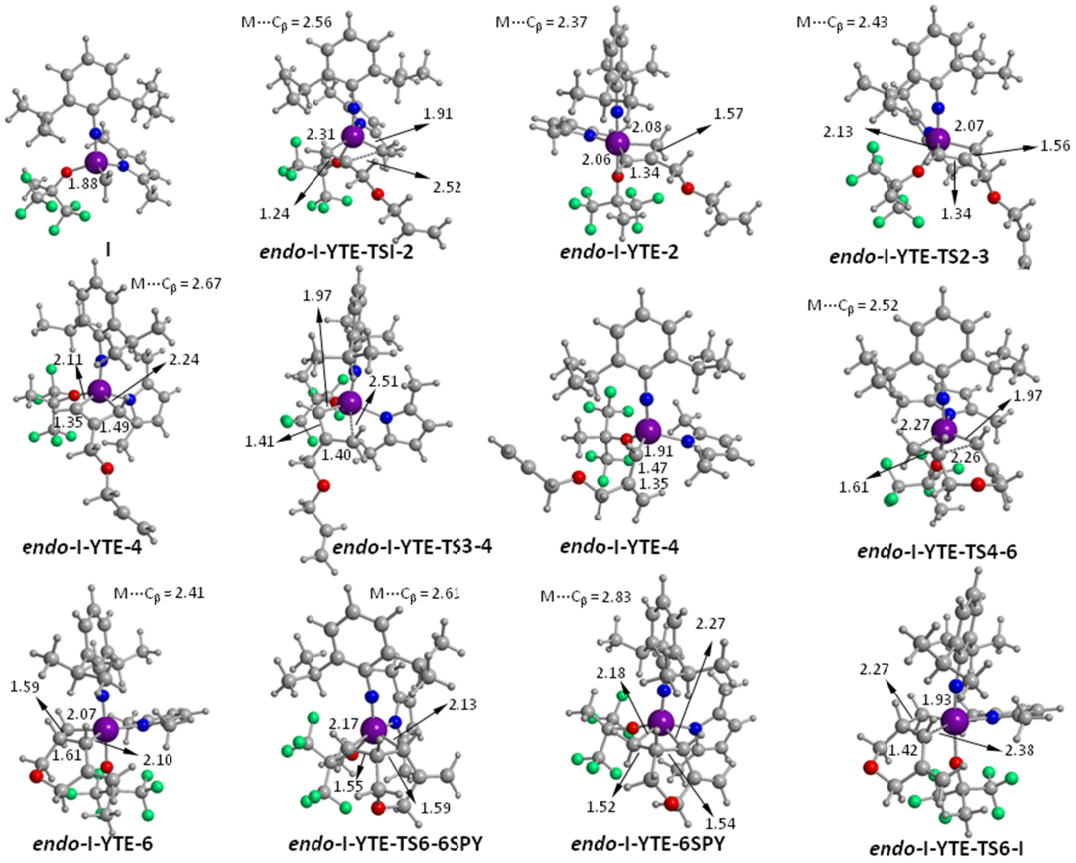

Figure 3. Optimized geometries of all intermediates and transtion structures involved in the reaction of alkylidene **I** with **R1** through the *endo-yne-then-ene* pathway.

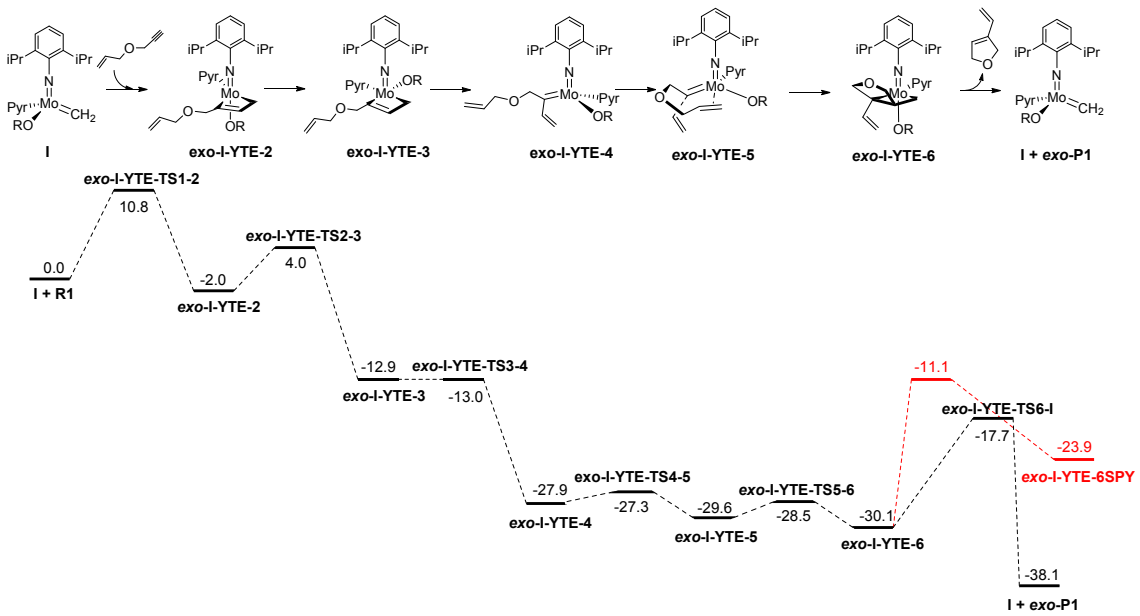

Figure 4. Gibbs energy profile (based on G_{gp}+ ΔG_{solv} + D in kcal mol^{-1}) for the reaction of alkylidene **I** with **R1** through the *exo-yne-then-ene* pathway.

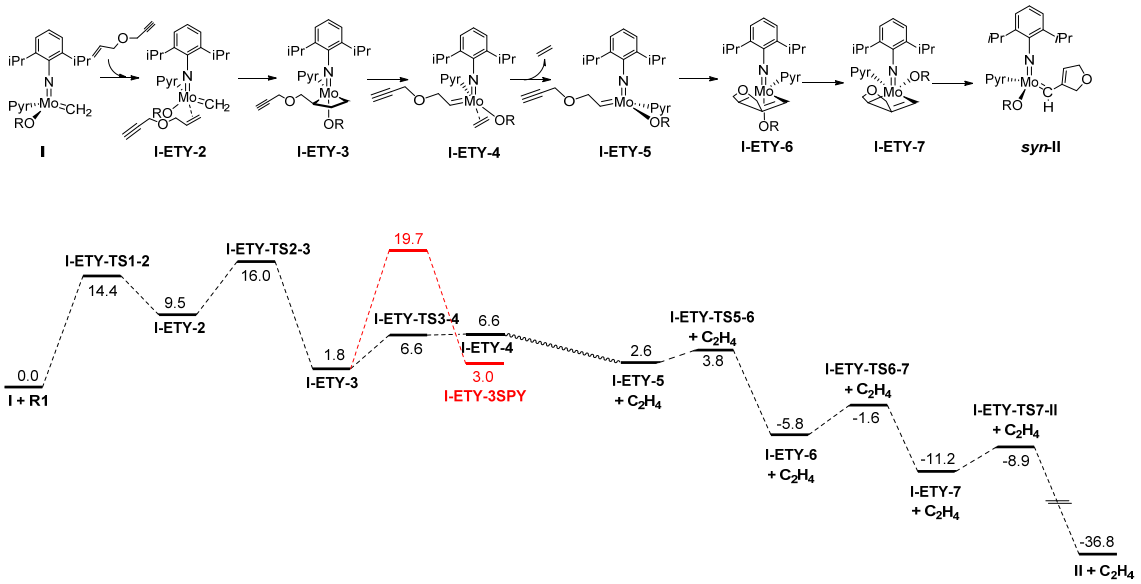

Figure 5. Gibbs energy profile (based on G_{gp}+ ΔG_{solv} + D in kcal mol^{-1}) for the reaction of alkylidene **I** with **R1** through the *ene-then-yne* pathway. This pathway interconverts the two potentially active alkylidene species.

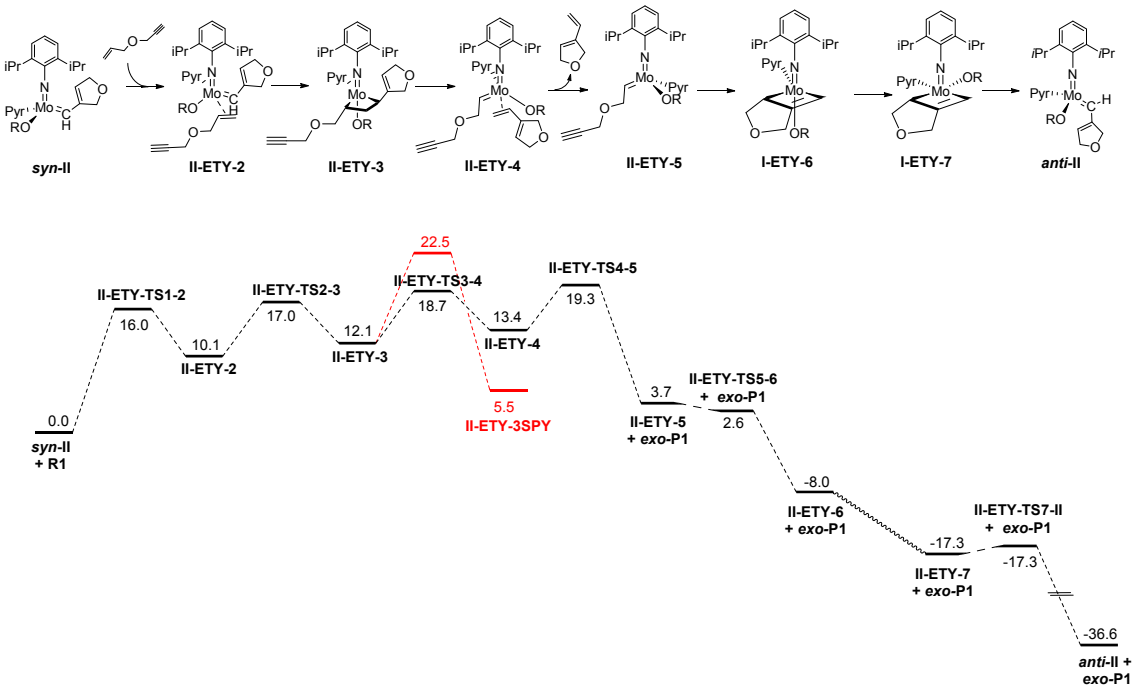

Figure 6. Gibbs energy profile (based on G_{gp}+ ΔG_{solv} + D in kcal mol^{-1}) for the reaction of alkylidene **II** with **R1** through the *ene-then-yne* pathway.

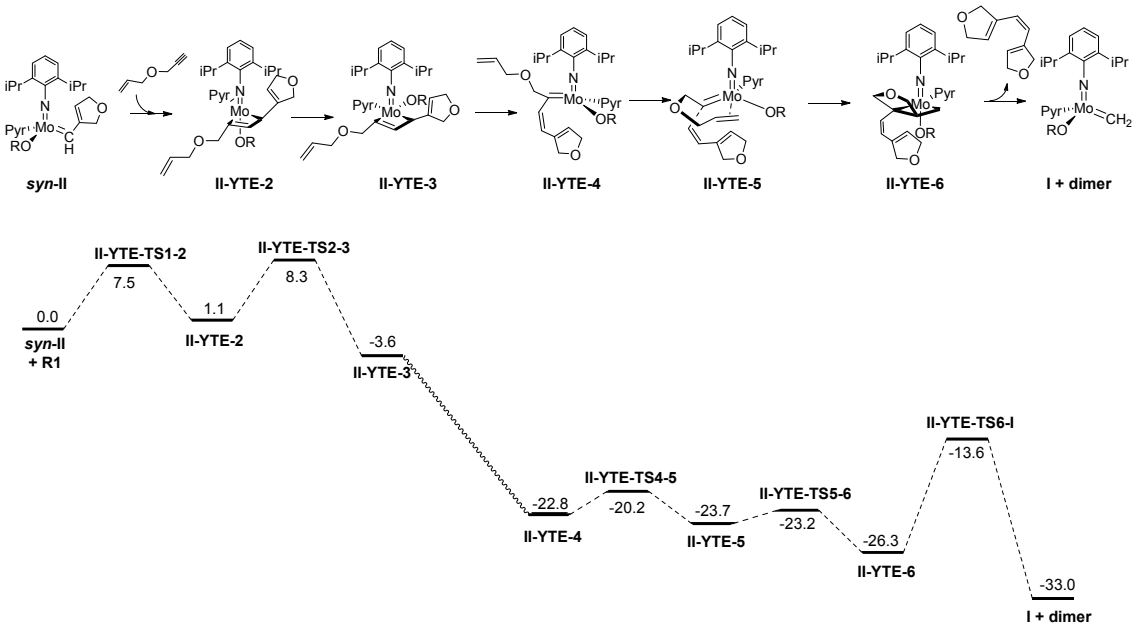

Figure 7. Gibbs energy profile (based on G_{gp}+ ΔG_{solv} + D in kcal mol^{-1}) for the reaction of alkylidene **II** with **R1** through an *yne-then-ene* pathway. This pathway leads to the formation of dimeric species.

REFERENCES

1. A. Kinoshita and M. Mori, *Synlett.*, 1994, 1020-1022.
2. S. T. Diver, *Coord. Chem. Rev.*, 2007, **251**, 671-701.
3. T. J. Katz and T. M. Sivavec, *J. Am. Chem. Soc.*, 1985, **107**, 737-738.
4. S. T. Diver and A. J. Giessert, *Chem. Rev.*, 2004, **104**, 1317-1382.
5. N. Calderon, H. Y. Chen and K. W. Scott, *Tetrahedron Lett.*, 1967, **8**, 3327-3329.
6. J. C. Mol, *J. Mol. Catal. A: Chem.*, 2004, **213**, 39-45.
7. R. R. Schrock, *Angew. Chem. Int. Ed.*, 2006, **45**, 3748-3759.
8. R. R. Schrock, *Chem. Rev.*, 2009, **109**, 3211-3226.
9. R. H. Grubbs, *Angew. Chem. Int. Ed.*, 2006, **45**, 3760-3765.
10. G. C. Vougioukalakis and R. H. Grubbs, *Chem. Rev.*, 2010, **110**, 1746-1787.
11. Y. Chauvin, *Angew. Chem. Int. Ed.*, 2006, **45**, 3740-3747.
12. P. H. Deshmukh and S. Blechert, *Dalton Trans.*, 2007, 2479-2491.
13. A. Fürstner, *Angew. Chem. Int. Ed.*, 2000, **39**, 3013-3043.
14. K. C. Nicolaou, P. G. Bulger and D. Sarlah, *Angew. Chem. Int. Ed.*, 2005, **44**, 4490-4527.
15. A. H. Hoveyda and A. R. Zhugralin, *Nature*, 2007, **450**, 243-251.
16. M. Mori, *Adv. Synth. Catal.*, 2007, **349**, 121-135.
17. H. Villar, M. Frings and C. Bolm, *Chem. Soc. Rev.*, 2007, **36**, 55-66.
18. A. Deiters and S. F. Martin, *Chem. Rev.*, 2004, **104**, 2199-2238.
19. M. Mori, N. Sakakibara and A. Kinoshita, *J. Org. Chem.*, 1998, **63**, 6082-6083.
20. Y. J. Lee, R. R. Schrock and A. H. Hoveyda, *J. Am. Chem. Soc.*, 2009, **131**, 10652-10661.
21. Y. Zhao, A. H. Hoveyda and R. R. Schrock, *Org. Lett.*, 2011, **13**, 784-787.
22. R. Singh, R. R. Schrock, P. Müller and A. H. Hoveyda, *J. Am. Chem. Soc.*, 2007, **129**, 12654-12655.
23. V. Sashuk and K. Grela, *J. Mol. Catal. A: Chem.*, 2006, **257**, 59-66.

24. G. C. Lloyd-Jones, R. G. Margue and J. G. De Vries, *Angew. Chem. Int. Ed.*, 2005, **44**, 7442-7447.

25. T. Kitamura, Y. Sato and M. Mori, *Chem. Commun.*, 2001, 1258-1259.

26. T. Kitamura, Y. Sato and M. Mori, *Adv. Synth. Catal.*, 2002, **344**, 678-693.

27. A. G. D. Grotevendt, J. A. M. Lummiss, M. L. Mastronardi and D. E. Fogg, *J. Am. Chem. Soc.*, 2011, **133**, 15918-15921.

28. J. A. Love, M. S. Sanford, M. W. Day and R. H. Grubbs, *J. Am. Chem. Soc.*, 2003, **125**, 10103-10109.

29. M. S. Sandford, J. A. Love and R. H. Grubbs, *J. Am. Chem. Soc.*, 2001, **123**, 6543-6554.

30. V. Thiel, M. Hendann, K. J. Wannowius and H. Plenio, *J. Am. Chem. Soc.*, 2012, **134**, 1104-1114.

31. I. W. Ashworth, I. H. Hillier, D. J. Nelson, J. M. Percy and M. A. Vincent, *Chem. Commun.*, 2011, **47**, 5428-5430.

32. J. S. Kingsbury and A. H. Hoveyda, *J. Am. Chem. Soc.*, 2005, **127**, 4510-4517.

33. N. Dieltiens, K. Moonen and C. V. Stevens, *Chem. Eur. J.*, 2007, **13**, 203-214.

34. T. R. Hoye, S. M. Donaldson and T. J. Vos, *Org. Lett.*, 1999, **1**, 277-279.

35. O. S. Lee, K. H. Kim, J. Kim, K. Kwon, T. Ok, H. Ihee, H. Y. Lee and J. H. Sohn, *J. Org. Chem.*, 2013, **78**, 8242-8249.

36. K. H. Kim, T. Ok, K. Lee, H. S. Lee, K. T. Chang, H. Ihee and J. H. Sohn, *J. Am. Chem. Soc.*, 2010, **132**, 12027-12033.

37. H. Y. Lee, B. Gyu Kim and M. L. Snapper, *Org. Lett.*, 2003, **5**, 1855-1858.

38. E. C. Hansen and D. Lee, *Acc. Chem. Res.*, 2006, **39**, 509-519.

39. C. Adlhart and P. Chen, *Angew. Chem. Int. Ed.*, 2002, **41**, 4484-4487.

40. L. Cavallo, *J. Am. Chem. Soc.*, 2002, **124**, 8965-8973.

41. S. F. Vyboishchikov, M. Bühl and W. Thiel, *Chem. Eur. J.*, 2002, **8**, 3962-3975.

42. C. Adlhart and P. Chen, *J. Am. Chem. Soc.*, 2004, **126**, 3496-3510.

43. B. F. Straub, *Angew. Chem. Int. Ed.*, 2005, **44**, 5974-5978.

44. J. J. Lippstreu and B. F. Straub, *J. Am. Chem. Soc.*, 2005, **127**, 7444-7457.

45. A. Correa and L. Cavallo, *J. Am. Chem. Soc.*, 2006, **128**, 13352-13353.

46. G. Occhipinti, H. R. Bjørsvik and V. R. Jensen, *J. Am. Chem. Soc.*, 2006, **128**, 6952-6964.

47. R. García-Fandiño, L. Castedo, J. R. Granja and D. J. Cárdenas, *Dalton Trans.*, 2007, 2925-2934.

48. V. Zhao and D. G. Truhlar, *Org. Lett.*, 2007, **9**, 1967-1970.

49. D. Benitez, E. Tkatchouk and W. A. Goddard III, *Chem. Commun.*, 2008, 6194-6196.

50. H. Clavier, A. Correa, E. C. Escudero-Adán, B. B. Jordi, L. Cavallo and S. P. Nolan, *Chem. Eur. J.*, 2009, **15**, 10244-10254.

51. Y. Minenkov, G. Occhipinti and V. R. Jensen, *J. Phys. Chem. A*, 2009, **113**, 11833-11844.

52. X. Solans-Monfort, R. Pleixats and M. Sodupe, *Chem. Eur. J.*, 2010, **16**, 7331-7343.

53. F. Nuñez-Zarur, X. Solans-Monfort, L. Rodríguez-Santiago and M. Sodupe, *Organometallics*, 2012, **31**, 4203-4215.

54. P. Liu, X. Xu, X. Dong, B. K. Keitz, M. B. Herbert, R. H. Grubbs and K. N. Houk, *J. Am. Chem. Soc.*, 2012, **134**, 1464-1467.

55. F. Núñez-Zarur, X. Solans-Monfort, R. Pleixats, L. Rodríguez-Santiago and M. Sodupe, *Chem. Eur. J.*, 2013, **19**, 14553-14565.

56. A. K. Rappé and W. A. Goddard III, *J. Am. Chem. Soc.*, 1982, **104**, 448-456.

57. E. Folga and T. Ziegler, *Organometallics*, 1993, **12**, 325-337.

58. Y. D. Wu and Z. H. Peng, *J. Am. Chem. Soc.*, 1997, **119**, 8043-8049.

59. T. P. M. Goumans, A. W. Ehlers and K. Lammertsma, *Organometallics*, 2005, **24**, 3200-3206.

60. A. Poater, X. Solans-Monfort, E. Clot, C. Copéret and O. Eisenstein, *Dalton Trans.*, 2006, 3077-3087.

61. J. Zhu, G. Jia and Z. Lin, *Organometallics*, 2006, **25**, 1812-1819.

62. S. Beer, C. G. Hrib, P. G. Jones, K. Brandhorst, J. Grunenberg and M. Tamm, *Angew. Chem. Int. Ed.*, 2007, **46**, 8890-8894.

63. A. Poater, X. Solans-Monfort, E. Clot, C. Copéret and O. Eisenstein, *J. Am. Chem. Soc.*, 2007, **129**, 8207-8216.

64. S. Beer, K. Brandhorst, C. G. Hrib, W. Xian, B. Haberlag, J. Grunenberg, P. G. Jones and M. Tamm, *Organometallics*, 2009, **28**, 1534-1545.

65. B. Haberlag, X. Wu, K. Brandhorst, J. Grunenberg, C. G. Daniliuc, P. G. Jones and M. Tamm, *Chem. Eur. J.*, 2010, **16**, 8868-8877.

66. X. Solans-Monfort, C. Copéret and O. Eisenstein, *J. Am. Chem. Soc.*, 2010, **132**, 7750-7757.

67. X. Solans-Monfort, C. Copéret and O. Eisenstein, *Organometallics*, 2012, **31**, 6812-6822.

68. C. Wang, F. Haeffner, R. R. Schrock and A. H. Hoveyda, *Angew. Chem. Int. Ed.*, 2013, **52**, 1939-1943.

69. X. Solans-Monfort, E. Clot, C. Copéret and O. Eisenstein, *J. Am. Chem. Soc.*, 2005, **127**, 14015-14025.

70. X. Solans-Monfort, E. Clot, C. Copéret and O. Eisenstein, *Organometallics*, 2005, **24**, 1586-1597.

71. A. M. Leduc, A. Salameh, D. Soulivong, M. Chabanas, J. M. Basset, C. Copéret, X. Solans-Monfort, E. Clot, O. Eisenstein, V. P. W. Böhm and M. Röper, *J. Am. Chem. Soc.*, 2008, **130**, 6288-6297.

72. J. L. Hérisson and Y. Chauvin, *Makromol. Chem.*, 1970, **141**, 161-176.

73. R. R. Schrock, R. T. DePue, J. Feldman, C. J. Schaverien, J. C. Dewan and A. H. Liu, *J. Am. Chem. Soc.*, 1988, **110**, 1423-1435.

74. J. Feldman, J. S. Murdzek, W. M. Davis and R. R. Schrock, *Organometallics*, 1989, **8**, 2260-2265.

75. J. Feldman, W. M. Davis and R. R. Schrock, *Organometallics*, 1989, **8**, 2266-2268.

76. J. Feldman, W. M. Davis, J. K. Thomas and R. R. Schrock, *Organometallics*, 1990, **9**, 2535-2548.

77. F. Blanc, R. Berthoud, C. Copéret, A. Lesage, L. Emsley, R. Singh, T. Kreickmann and R. R. Schrock, *Proc. Natl. Acad. Sci. USA*, 2008, **105**, 12123-12127.

78. R. R. Schrock, A. J. Jiang, S. C. Marinescu, J. H. Simpson and P. Müller, *Organometallics*, 2010, **29**, 5241-5251.

79. A. J. Jiang, J. H. Simpson, P. Müller and R. R. Schrock, *J. Am. Chem. Soc.*, 2009, **131**, 7770-7780.

80. T. J. Katz and J. McGinnis, *J. Am. Chem. Soc.*, 1975, **97**, 1592-1594.

81. F. Nuñez-Zarur, X. Solans-Monfort, L. Rodríguez-Santiago, R. Pleixats and M. Sodupe, *Chem. Eur. J.*, 2011, **17**, 7506-7520.

82. F. Nuñez-Zarur, X. Solans-Monfort, L. Rodríguez-Santiago and M. Sodupe, *ACS Catal.*, 2013, **3**, 206-218.

83. A. D. Becke, *J. Chem. Phys.*, 1993, **98**, 5648-5652.

84. C. Lee, W. Yang and R. G. Parr, *Phys. Rev. B*, 1988, **37**, 785-789.

85. M. M. Francl, W. J. Pietro, W. J. Hehre, J. S. Binkley, M. S. Gordon, D. J. DeFrees and J. A. Pople, *J. Chem. Phys.*, 1982, **77**, 3654-3665.

86. W. J. Hehre, K. Ditchfield and J. A. Pople, *J. Chem. Phys.*, 1972, **56**, 2257-2261.

87. W. Kuechle, M. Dolg, H. Stoll and H. Preuss, *Mol. Phys.*, 1991, **74**, 1245-1263.

88. A. W. Ehlers, M. Böhme, S. Dapprich, A. Gobbi, A. Höllwarth, V. Jonas, K. F. Köhler, R. Stegmann, A. Veldkamp and G. Frenking, *Chem. Phys. Lett.*, 1993, **208**, 111-114.

89. P. C. Hariharan and J. A. Pople, *Theor. Chim. Acta*, 1973, **28**, 213-222.

90. S. Miertus, E. Scrocco and J. Tomasi, *Chem. Phys.*, 1981, **55**, 117-129.

91. V. Barone and M. Cossi, *J. Phys. Chem. A*, 1998, **102**, 1995-2001.

92. M. Cossi, N. Rega, G. Scalmani and V. Barone, *J. Comput. Chem.*, 2003, **24**, 669-681.

93. P. Śliwa and J. Handzlik, *Chem. Phys. Lett.*, 2010, **493**, 273-278.

94. S. Grimme, *J. Comput. Chem.*, 2004, **25**, 1463-1473.

95. S. Grimme, *J. Comput. Chem.*, 2006, **27**, 1787-1799.

96. M. J. Frisch, G. W. Trucks, H. B. Schlegel, G. E. Scuseria, M. A. Robb, J. R. Cheeseman, J. Montgomery, J. A., T. Vreven, K. N. Kudin, J. C. Burant, J. M. Millam, S. S. Iyengar, J. Tomasi, V. Barone, B. Mennucci, M. Cossi, G. Scalmani, N. Rega, G. A. Petersson, H. Nakatsuji, M. Hada, M. Ehara, K. Toyota, R. Fukuda, J. Hasegawa, M. Ishida, T. Nakajima, Y. Honda, O. Kitao, H. Nakai, M. Klene, X. Li, J. E. Knox, H. P. Hratchian, J. B. Cross, V. Bakken, C. Adamo, J. Jaramillo, R. Gomperts, R. E. Stratmann, O. Yazyev, A. J. Austin, R. Cammi, C. Pomelli, J. W. Ochterski, P. Y. Ayala, K. Morokuma, G. A. Voth, P. Salvador, J. J. Dannenberg, V. G. Zakrzewski, S. Dapprich, A. D. Daniels, M. C. Strain, O. Farkas, D. K. Malick, A. D. Rabuck, K. Raghavachari, J. B. Foresman, J. V. Ortiz, Q. Cui, A. G. Baboul, S. Clifford, J. Cioslowski, B. B. Stefanov, G. Liu, A. Liashenko, P. Piskorz, I. Komaromi, R. L. Martin, D. J. Fox, T. Keith, M. A. Al-Laham, C. Y. Peng, A. Nanayakkara, M. Challacombe, P. M. W. Gill, B. Johnson, W. Chen, M. W. Wong, C. Gonzalez and J. A. Pople, *Gaussian03, Revision C.02*, (2004) Gaussian, Inc., Wallingford CT.

97. M. J. Frisch, G. W. Trucks, H. B. Schlegel, G. E. Scuseria, M. A. Robb, J. R. Cheeseman, G. Scalmani, V. Barone, B. Mennucci, G. A. Petersson, H. Nakatsuji, M. Caricato, X. Li, H. P. Hratchian, A. F. Izmaylov, J. Bloino, G. Zheng, J. L. Sonnenberg, M. Hada, M. Ehara, K. Toyota, R. Fukuda, J. Hasegawa, M. Ishida, T. Nakajima, Y. Honda, O. Kitao, H. Nakai, T. Vreven, J. A. Montgomery Jr., J. E. Peralta, F. Ogliaro, M. Bearpark, J. J. Heyd, E. Brothers, K. N. Kudin, V. N. Staroverov, R. Kobayashi, J. Normand, K. Raghavachari, A. Rendell, J. C. Burant, S. S. Iyengar, J. Tomasi, M. Cossi, N. Rega, N. J. Millam, M. Klene, J. E. Knox, J. B. Cross, V. Bakken, C. Adamo, J. Jaramillo, R. Gomperts, R. E. Stratmann, O. Yazyev, A. J. Austin, R. Cammi, C. Pomelli, J. W. Ochterski, R. L. Martin, K. Morokuma, V. G. Zakrzewski, G. A. Voth, P. Salvador, J. J. Dannenberg, S. Dapprich, A.

D. Daniels, Ö. Farkas, J. B. Foresman, J. V. Ortiz, J. Cioslowski and D. J. Fox, *Gaussian09, Revision D.01*, (2009) Gaussian, Inc., Wallingford CT.

98. Differences larger than 2.7 kcal mol^{-1} are sufficient to predict 99% selectivity for the product obtained through the most favorable pathway.

Table of Contents graphic:

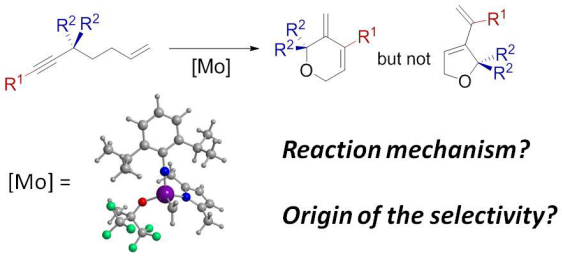

Table of Contents text: DFT calculations show that the RCEYM reaction catalyzed by Mo-based catalysts proceeds preferently through an yne-then-ene mechanism and that the *endo*-/*exo*- selectivity mainly depends on sterics.